

GT2011-46701

## EXPERIMENTAL ANALYSIS OF SIMULTANEOUS NON-HARMONICALLY RELATED UNSTABLE MODES IN A SWIRLED COMBUSTOR

Ammar Lamraoui, Franck Richecoeur, Sébastien Ducruix, Thierry Schuller

École Centrale Paris  
Laboratoire EM2C – CNRS  
Grande Voie des Vignes  
F-92295 Châtenay-Malabry  
Email: franck.richecoeur@em2c.ecp.fr

### ABSTRACT

*The present study investigates combustion instabilities generated in a turbulent swirled combustor featuring two non-harmonically related unstable modes. Sound pressure and chemiluminescence spectra show the presence of two peaks located around 180 Hz and 280 Hz during unstable operation. The low frequency acoustic response of the test-rig is then analyzed using a two-coupled-cavity model including a realistic impedance of the system at the premixer inlet. This analytical approach is used to link the two observed frequencies to the first chamber and premixer modes respectively. Analytical predictions are compared with acoustic pressure measurements to determine the structure of these modes. The Rayleigh source term in the energy balance is also computed and shows that the two modes feed acoustic energy simultaneously in the system. High-speed PIV data gathered under unstable operation are filtered around these two frequencies to obtain phase conditioned images. Results show that the unsteady flow in the flame region features distinct dynamics associated to a bulk longitudinal oscillation of the flow in the flame arms at 180 Hz and large wrinkles in the radial direction at 280 Hz.*

### 1 INTRODUCTION

The development of lean premixed burners for propulsion and energy production succeeded in reducing pollutant emissions like NO<sub>x</sub> by lowering the combustion temperature. While this process is efficient to satisfy legislative constraints, it is now

facing the problem of combustion instabilities and noise reduction. These phenomena originate in the coupling between acoustic pressure waves, the turbulent flow and unsteady heat release in a confined environment. The problem can be analyzed by examining the acoustic energy balance in a low Mach flow [1]:

$$\frac{\partial \mathcal{E}}{\partial t} + \nabla \cdot (p_1 \mathbf{u}_1) = \frac{\gamma - 1}{\gamma p_0} p_1 \dot{q}_1 \quad (1)$$

where  $\mathcal{E} = p_1^2 / (2\rho_0 c^2) + (\rho_0 u_1^2) / 2$  is the acoustic energy density,  $p_1$ ,  $u_1$  and  $\dot{q}_1$  indicate respectively the acoustic pressure, velocity and the heat release rate fluctuations,  $p_0$  is the mean pressure and  $\gamma$  is the specific heat capacity ratio. If the Rayleigh source term (r.h.s. term) and the acoustic fluxes at the boundaries (second l.h.s. term) differ in such a way that the net effect is a positive contribution, an accumulation of acoustic energy may then be observed in the system. Budgets for energy flow disturbances have received much attention to include mean flow, entropy or vorticity effects to generalize the acoustic energy balance in more complex flows [2–7]. Experimental validations leading to quantitative results are less common and they generally consider only the main contributions appearing in Eq. (1). This was for example carried out by Tran et al. [8] to show that the predominant flux counterbalancing the Rayleigh source term in a swirled test rig open to atmospheric conditions was associated to the upstream acoustic flux. This type of analysis requires a detailed characterization of all impedances in the combustor [9–14]. This is generally too difficult in complex chamber geometries and only

the Rayleigh source term is considered in many studies.

The Rayleigh source term integrated over the reaction zone volume indicates when unsteady combustion interacts positively with pressure waves to sustain the instability. It is generally examined at one single frequency corresponding to the main oscillation peak frequency observed in the combustor (see for example Refs. [15] and [16] for quantitative evaluations of the different terms in the acoustic energy budget in unconfined configurations or in a turbulent swirled burner respectively). There are also cases with multiple unstable modes. This situation was recently discussed by Moeck and Paschereit [17] in an analysis of nonlinear interactions between unstable modes. These authors mentioned that multiple unstable modes are not uncommon in thermoacoustic systems, but that it is in most cases simpler to identify this phenomenon in model simulations [18, 19] than in test-rig experiments. Multiple peaks at non-harmonically related frequencies in pressure spectra were explicitly mentioned in several studies (see among others [20–22]), but only a few [23, 24] clearly indicate the simultaneous presence of multiple frequencies under unstable operation for the same operating conditions. Experiments conducted by Noiray *et al.* [25], Boudy *et al.* [26] show for example that the system may switch between two eigenmodes and eventually switch back again to the first mode [17], but these modes are not present simultaneously.

There is to date no detailed investigation of the flame response in a configuration featuring two self-sustained modes at non-harmonically related frequencies. Balanchandran *et al.* [27] considered the response of a swirled flames to flow modulations at two simultaneous forcing frequencies, the second frequency being an harmonic of the first one. They showed that this results in perturbations of the vortex shedding synchronization in the shear layers of the swirled flame and this modifies in turn the flame transfer function. When non-harmonic multiple frequencies are considered, it is not clear whether the same elementary mechanisms are responsible for heat release rate perturbations at the different discrete frequencies involved. It is for example known that different mechanisms may generate large heat release rate fluctuations, but they are generally frequency dependent [28].

An experimental analysis is conducted to gain more insight into swirled flame dynamics featuring multiple simultaneous unstable modes. The configuration explored here is described in the next section together with the operating conditions leading to a self-sustained oscillation state characterized by two unstable frequencies. An acoustic analysis of the test rig is then conducted to identify the corresponding acoustic modes associated to the two unstable frequencies in section 3. The acoustic/flow/flame coupling is then analyzed in section 4 combining acoustic pressure, chemiluminescence emission from the flame together with high speed Particle Imaging Velocimetry (PIV) measurements. The flow and flame responses are analyzed at the two unstable frequencies by post-processing the data

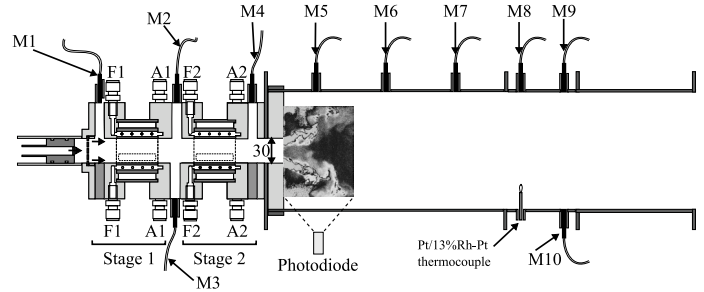


**FIGURE 1.** CESAM test bench fed with propane and air through two identical stages. The locations of microphones M1 to M10, the photodiode and the thermocouple are also indicated.

around these frequencies. Some conclusions and perspectives are finally given on the potential mechanisms governing the flame response at these distinct frequencies.

## 2 CESAM TEST BENCH AND DIAGNOSTICS

The experimental setup CESAM features a partially pre-mixed burner consisting of two identical stages through which air is injected tangentially (Fig. 1). The internal geometry of the combustor stage is also shown in Fig. 2. Propane is injected through small slits, 1 mm in diameter mounted perpendicular to the air flow. Each stage is equipped with 8 propane injection holes. The small size of these injectors enables to inject propane at high speed, limiting the risks of flashback in the injection lines. This is also beneficial for the premixing of the reactants. Tangential injection of air generates a swirling flow in the premixing tube of 30 mm in diameter. The presence of a strong internal recirculation zone indicates a swirl number  $S$  larger than 0.6 [29]. A small fraction of the air corresponding to less than 2.5 % of the total mass flow is injected through the backplane at the rear side of the premixer to avoid flashback in the injection lines. The premixer is also equipped with an Impedance Control System (ICS) described in [8] that can be used to modify the combustor inlet impedance. In the present study, this inlet acoustic impedance was kept constant. Air and propane are regulated by mass flow controllers (Bronkhorst EL-FLOW) in each stage. The fuel and air feeding lines are then split into two branches, with similar lengths of about 1.95 m. These lines are connected to the injection stages of the combustor by four main inputs, two for air and two for propane, to put the flow in rotation.

The premixer unit is connected to a combustion chamber of square section  $10 \times 10 \text{ cm}^2$ , the top and bottom faces are made of refractory concrete while the side walls are made of quartz to allow visualization of the flame and use of optical diagnostics. The chamber length is 88 cm and is opened to atmospheric conditions where a collector is installed to vent the hot gases to

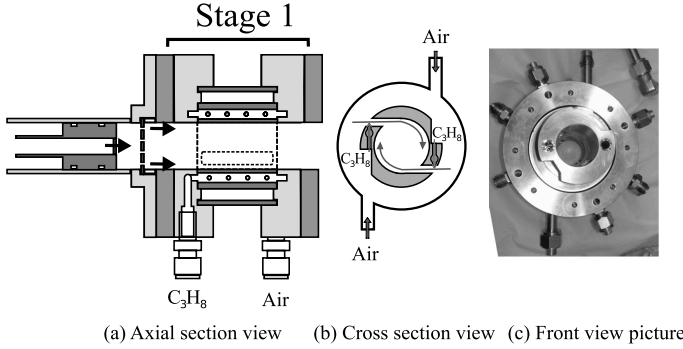


**FIGURE 2.** Different sectional views of the internal geometry of the combustor first fuel and air injection stage.

**TABLE 1.** Parameters used to run the experiment in the present study

Air mass flow rate	Fuel mass flow rate	Equivalence ratio	Staging	Power
[g/s]	[g/s]		[%]	[kW]
14.8	0.8	0.82	48	36

a chimney. Microphones installed in water-cooled waveguides are used to determine the structure of the acoustic field inside the combustor. Microphones M1 to M3 were also used to determine the premixer inlet impedance and M8 to M10 the outlet impedance the combustion chamber. The flame is stabilized in the swirling flow by a central recirculating zone and by the recirculation of hot gases at the chamber dump plane. This leads to a compact V-flame with a length of approximately 15 cm characteristic of swirl stabilized flames. The combustor was designed to study low frequency thermo-acoustic instabilities in lean premixed regimes for thermal powers ranging from 35 to 55 kW. In the frequency range 0 – 1000 Hz only longitudinal acoustic modes can develop given the dimensions of the test rig.

The staging  $\alpha$  defines the proportion of fuel injected through the first stage compared to the total fuel mass flow rate:

$$\alpha = \frac{\dot{m}_{C_3H_8}^{(1)}}{\dot{m}_{C_3H_8}^{(1)} + \dot{m}_{C_3H_8}^{(2)}}$$

This parameter can be varied between 0.1 and 0.60, limitations come from flashback risks. In the present study, the staging, the equivalence ratio and the air and propane mass flow rates are kept constant. The operating point parameters are listed in Tab 1.

The combustor is equipped with microphones for acoustic pressure measurements and photodiodes or photomultipliers equipped with filters for CH\* or OH\* spontaneous emission

measurements. All the microphones are B & K type 4938 1/4 inch. They operate over a frequency range from 4 Hz to 70 kHz and for sound pressure levels comprised between 30 and 172 dB in flows up to 450 K. In the combustion chamber, the temperature is much higher than their acceptable limit value, so the microphones are mounted on water-cooled waveguides with a long extension tube (about 16 m) where the waves dissipate slowly, avoiding reflection issues. This system introduces a time lag which corresponds to the travel time of sound waves from the wall orifice to the position where the measurement is done. Using a calibration procedure of these waveguides in the frequency range 0-1000 Hz, all measurements can be synchronized. The signals were sampled in this study with a duration of 8 s at a sampling frequency  $f_s = 16384$  Hz to ensure statistical convergence for spectral analysis. Figure 1 presents the bench equipped with different microphones (the waveguides are not represented in this figure), including four in the premixer unit (M1-M4) and three in the chamber (M5-M7). These microphones enable to describe accurately the acoustic pressure field inside the chamber for all unstable operating conditions.

The second type of diagnostic used on the bench are the optical measurements of CH\* and OH\* chemiluminescence. Photodiodes or photomultipliers are equipped with filters centered on wavelengths  $\lambda_1 = 430 \pm 10$  nm and  $\lambda_2 = 310 \pm 30$  nm to record CH\* and OH\* emissions respectively. These systems are mounted in front of the quartz windows pointing towards the flame zone. Converging quartz lenses (Melles Griot, 15 cm in diameter and focal lengths  $f = 300$  mm and  $f = 430$  mm) are used to focus light emanating from the chamber to the sensors equipped with the filters.

Finally, high-speed PIV measurement campaigns are conducted to examine the unsteady flow motion under unstable operation. To this purpose, top and bottom walls of the chamber are equipped with quartz windows allowing the laser sheet to cross the chamber. Zirconium oxide particles are used to seed the flow enabling measurements of the velocity fields both in the fresh and burnt gases regions. Two laser sheets are generated using two Nd:YAG lasers running at 15 kHz, emitting pulses at 532 nm, with an energy of about 6 mJ and a duration of 160 ns. A high speed camera is focused on the flame, with a frame rate of 30 kHz. At this resolution, the region of interest contains  $448 \times 504$  pixels representing  $45 \times 52$  mm<sup>2</sup> and the signal is recorded during 0.85 s.

### 3 ACOUSTIC ANALYSIS

For the operating point considered in Tab. 1 corresponding to a thermal power of 36 kW, the combustion features a self-sustained oscillation characterized by an acoustic signature presented in Fig. 3. The power spectral densities of the acoustic pressure measured by microphone M3 in the premixer and microphone M5 placed in the chamber in front of the reaction zone fea-

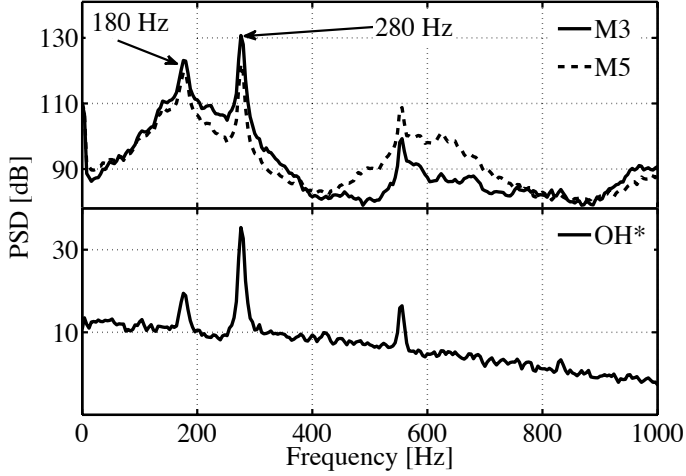


**FIGURE 3.** Power Spectral Densities of acoustic pressure measured by microphones M3 and M5 and of the OH\* chemiluminescence signal. Two dominant peaks can be observed at 180 and 280 Hz.

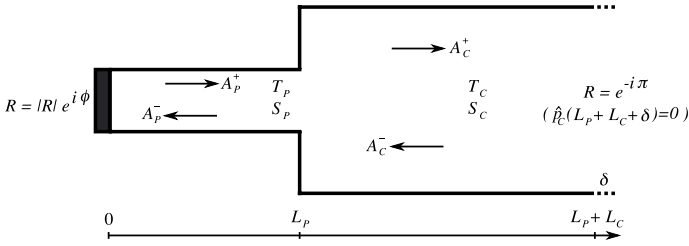


**FIGURE 4.** Model of the combustor used to determine the acoustic modes.

ture distinct peak frequencies at  $f = 180, 280$  and  $556$  Hz above a noisy continuous background. These peaks are also present in the power spectrum of the OH\* emission signal of the flame, which clearly indicates that a resonant coupling takes place between the unsteady combustion and the combustor acoustics for this operating condition at multiple unstable frequencies. The structure of the corresponding acoustic field is now investigated using an analytical model.

Figure 4 represents a schematic view of the acoustic model used to determine the combustor modes. It comprises two cavities, the subscripts  $p$  and  $c$  indicating the premixing tube and the chamber, respectively. The lengths of the premixing tube and the combustion chamber are  $L_p = 235$  mm and  $L_c = 880$  mm. To take into account the open termination of the chamber, the chamber length is corrected by adding the length  $\delta = 0.85D_h/2$  where  $D_h$  is the hydraulic diameter of the square cross section [30]. All variables are written as a sum of a mean and a fluctuating component  $x = \bar{x} + x'$ , where the disturbances are regarded as harmonics

$$x' = \hat{x}e^{-i\omega t} \text{ and } \omega = 2\pi f.$$

The temperature in the premixer is fixed to  $T_p = 300$  K in the model and the temperature of the gas filling the combustion chamber is assumed uniform and constant at about  $T_c = 1200$  K. This is an average value of the flue gases temperature measured at different locations inside the combustor with a thermocouple. The quantities  $\bar{c}_p$  and  $\bar{c}_c$  denote the speed of sound in the premixer and chamber respectively. PIV measurements described later show that the maximum velocity  $25 \text{ m s}^{-1}$  is reached in the fresh reactant, in the penetration cone of the swirling flow. This corresponds to a maximum Mach number  $M = 0.07$ , implying that convective effects in the premixer and the chamber can be neglected in this test rig [7].

The present study focuses on low frequency thermo-acoustic instabilities (below 1 kHz). Below the cutoff frequency of the premixer and the chamber, only plane waves propagate in the combustor. The premixing tube features a cylindrical section with a radius  $r_p$ , which cutoff frequency is given by  $f_p^{\text{cut}} = 1.84c_p/2\pi r_p = 6774$  Hz at  $T_p = 300$  K. The combustion chamber features a square cross section yielding a cutoff frequency given by  $f_c^{\text{cut}} = \bar{c}_c/2h$  where  $h$  is the side length. At  $T_c = 300$  K,  $f_c^{\text{cut}} = 1826$  Hz while  $f_c^{\text{cut}} = 3542$  Hz at  $T_c = 1200$  K. This confirms that only planar acoustic waves propagate in the combustor in the frequency range considered here.

The acoustic field in the two cavities shown in Fig. 4 results from the superposition of waves propagating in the downstream and upstream directions. Introducing the notations  $Z_p = \bar{\rho}_p \bar{c}_p$  and  $Z_c = \bar{\rho}_c \bar{c}_c$  for the characteristic impedances of the gas in the premixing tube and the combustion chamber respectively, the acoustic field is then given by the set of equations:

$$\hat{p}_p(x) = A_p^+ e^{ik_p x} + A_p^- e^{-ik_p x} \quad (2)$$

$$Z_p \hat{u}_p(x) = A_p^+ e^{ik_p x} - A_p^- e^{-ik_p x} \quad (3)$$

$$\hat{p}_c(x) = A_c^+ e^{ik_c x} + A_c^- e^{-ik_c x} \quad (4)$$

$$Z_p \hat{u}_c(x) = A_c^+ e^{ik_c x} - A_c^- e^{-ik_c x} \quad (5)$$

where the wavenumber  $k_i = \omega/\bar{c}_i$  differs in the premixer  $i = p$  and the chamber  $i = c$ . The presence of hot gases is taken into account in the analysis by considering their temperature, but the presence of the flame as an active element is not considered.

This acoustic field must also comply with continuity relations and boundary conditions at the combustor inlet and outlet, which are defined by (i) the acoustic reflection coefficient  $R(0) = R_0 e^{i\phi}$  at the backplane of the premixer, (ii) the continuity of the acoustic pressure and the acoustic volume flow rate at the dump plate location and (iii) the acoustic pressure that vanishes

at the combustor outlet (Fig. 4):

$$A_p^+ = R_0 e^{i\phi} A_p^- \quad (6)$$

$$\hat{p}_p(L_p) = \hat{p}_c(L_p) \quad (7)$$

$$S_p \hat{u}_p(L_p) = S_c \hat{u}_c(L_p) \quad (8)$$

$$\hat{p}_c(L_p + L_c + \delta) = 0 \quad (9)$$

The acoustic modes of the system are given by the solutions of the dispersion equation:

$$(1 + \Xi) \left[ R(0) e^{i(k_p L_p + k_c L_c)} + e^{-i(k_p L_p + k_c L_c)} \right] + (1 - \Xi) \left[ R(0) e^{i(k_p L_p - k_c L_c)} + e^{-i(k_p L_p - k_c L_c)} \right] = 0 \quad (10)$$

where the dimensionless number  $\Xi$  is defined by:

$$\Xi = \frac{S_p \bar{\rho}_p \bar{c}_p}{S_c \bar{\rho}_c \bar{c}_c} = \frac{S_p}{S_c} \sqrt{\frac{T_p}{T_c}} \quad (11)$$

This interaction parameter characterizes the strength of the acoustic coupling between the two cavities. A small value indicates that the modes of the two cavities can be calculated separately. The solutions of the dispersion relation Eq. (10) yield the mode frequencies  $f_{pc}^n$ ,  $n \in \mathbb{N}$  of the combustor. The corresponding structure of the acoustic pressure in the pre-mixer and combustion chamber is given by the following expressions where the amplitudes were normalized by  $A_p^+ = 1$ :

$$\hat{p}_p(x) = R e^{ik_p x} + e^{-ik_p x} \quad \text{and} \quad (12)$$

$$\hat{p}_c(x) = \frac{1}{2}(1 + \Xi) \left[ R e^{i(k_p L_p + k_c(x-L_p))} + e^{-i(k_p L_p + k_c(x-L_p))} \right] + \frac{1}{2}(1 - \Xi) \left[ R e^{i(k_p L_p - k_c(x-L_p))} + e^{-i(k_p L_p - k_c(x-L_p))} \right] \quad (13)$$

Depending on the values of the interaction parameter  $\Xi$  and the inlet reflection coefficient  $R(0)$ , solutions of the dispersion equation may yield real angular frequencies  $\omega = 2\pi f$  or complex frequencies  $\omega = 2\pi f + i\omega_i$ , where  $\omega_i$  denotes the mode damping rate. Given the relatively high value of the gases temperature in the combustion chamber compared to that in the premixing tube and the large area expansion ratio between these two elements, the parameter  $\Xi$  often takes small values compared to 1. For  $T_c = 1200$  K, it is here equal to  $\Xi = 0.038$ . It is then interesting to

compare the first modes of the coupled cavities ( $f_{pc}^0, f_{pc}^1$ ) which are solution of Eq. (10) to those obtained by setting  $\Xi = 0$  in this equation. These solutions are denoted  $f_p^i$  and  $f_c^i$  corresponding to the  $i$ -th eigenfrequency in the premixing tube and chamber respectively.

Ideally, the boundary condition at the premixing tube back-plane  $x = 0$  corresponds to a rigid wall. In this case, the acoustic reflection coefficient takes a real value  $R(0) = 1$  and the dispersion relation Eq. (10) becomes:

$$\cos(k_p L_p) \cos(k_c L_c) - \Xi \sin(k_p L_p) \sin(k_c L_c) = 0 \quad (14)$$

In the limit of vanishingly small values of  $\Xi$ , the pre-mixer and chamber modes are decoupled and are given by :

$$\cos(k_p L_p) \cos(k_c L_c) = 0 \quad (15)$$

This equation is satisfied if one of the two terms vanishes and this yields the mode frequencies associated with the pre-mixer and the combustion chamber lengths, respectively:

$$f_p^{n_p} = (2n_p + 1)\bar{c}_p/4L_p$$

$$f_c^{n_c} = (2n_c + 1)\bar{c}_c/4L_c$$

These two sets of modes correspond to quarter-wave modes where  $(n_p, n_c) \in \mathbb{N}^2$ . Predictions for the first modes  $f_c^0, f_p^0$  calculated with  $\Xi = 0$  and  $f_{pc}^0$  and  $f_{pc}^1$  obtained for  $\Xi = 0.038$  are listed in Tab. 2 together with experimental data for the peak oscillation frequencies under unstable operation. In the first line, predictions are obtained for an inlet reflection coefficient  $R(0) = 1$  when the backplane of the pre-mixer corresponds to a rigid wall. It is first noted that the first mode of the coupled cavities matches well with the quarter-wave mode of the chamber  $f_{pc}^0 \simeq f_c^0$  and that the second mode of the coupled cavities is very close to the pure quarter-wave mode of the pre-mixer  $f_{pc}^1 \simeq f_p^0$ . This confirms that the pre-mixer and combustion chamber acoustic responses can be considered separately in this test rig. When these predictions are compared with the unstable oscillation peak frequencies observed in the combustor (first and last rows in Tab. 2), the first mode  $f_{pc}^0 = 186$  Hz associated to the chamber cavity is close to the lowest unstable frequency observed  $f = 180$  Hz. The second one  $f_{pc}^1 = 370$  Hz associated to the pre-mixer cavity lies however far away from the second unstable peak observed  $f = 280$  Hz.

The real impedance of the backplane of the pre-mixer must be taken into account. It cannot be considered as a rigid wall for acoustic waves since an air flow is injected through a set of perforations leading to slight modifications of the modulus and phase of the reflection coefficient  $R(0) = R_0 e^{i\phi}$ . This reflection coefficient has been measured under unstable operation using the three

**TABLE 2.** Eigenfrequencies of the system for coupled and uncoupled modes depending on the reflection coefficient at the premixing tube backplane (in Hz).

Inlet reflection coefficient	$\Xi = 0$		$\Xi = 0.038$	
	$f_c^0$	$f_p^0$	$f_{pc}^0$	$f_{pc}^1$
$R(0) = 1$	191	369	186	370
$R(0) = 0.8$	191	369	186	370
$R(0) = 0.8e^{i0.75}$	191	281	183	290
Experiment	×	×	180	280

microphones M1 to M3 and its evolution with the frequency is shown in Fig. 5. For frequencies higher than 400 Hz, the coherence between the microphones signals is too low to obtain reliable results [14]. For frequencies around 180 and 280 Hz, the modulus is found equal to  $|R(0)| = R_0 = 0.8$  and the phase is equal to  $\phi = 0.75$  rad. To investigate the effects of this inlet reflection coefficient, the dispersion relation Eq. (10) is solved by taking into account the measured values of  $R_0$  and  $\phi$ . This is done for  $\Xi = 0$  and  $\Xi = 0.038$  to obtain the uncoupled ( $f_c^0$ ,  $f_p^0$ ) and the coupled modes ( $f_{pc}^0$ ,  $f_{pc}^1$ ) respectively. The results of these calculations are summarized in the second and third lines of Tab 2.

This parametric analysis shows that the frequency  $f_{pc}^0$  associated to mode 1 is barely modified by modification of the pre-mixer inlet impedance. The reason is that mode 1 is essentially associated to the chamber cavity acoustics and is not very sensitive to the pre-mixer acoustic properties. The situation is different for the mode 2 characterized by a frequency  $f_{pc}^1$  which is mainly associated to the response of the pre-mixer. Thus, changing the pre-mixer inlet impedance strongly modifies the acoustic field in this region. As expected, the modulus of the reflection coefficient  $R_0$  barely changes the value of the eigenfrequency  $f_{pc}^1$ . This frequency is more sensitive to changes in the phase  $\phi$  of the reflection coefficient. Using the measured values of the reflection coefficient, it is now possible with the analytical model to recover the two unstable frequencies observed in the pressure spectrum.

The oscillation peak observed at 180 Hz is clearly associated to the chamber fundamental mode  $f_{pc}^0 \simeq f_c^0$  while the second unstable peak at 280 Hz is linked to the pre-mixer fundamental mode  $f_{pc}^1 \simeq f_p^0$ . This latter frequency is sensitive to slight variations in the phase of the pre-mixer inlet reflection coefficient  $R(0)$ . This can be confirmed by plotting the pressure distributions along the combustor for each mode identified. Results presented in Fig. 6 are normalized by the pressure fluctuation measured by microphone M<sub>1</sub>. The sound pressure measurements were also filtered around the two peak frequencies to extract their corresponding amplitude. Analytical predictions and acoustic pressure mea-

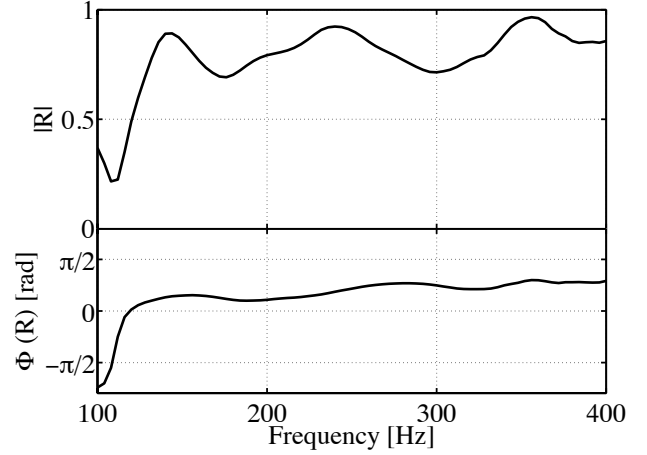


**FIGURE 5.** Modulus and phase of the reflection coefficient  $R(0)$  measured at the premixing tube backplane.

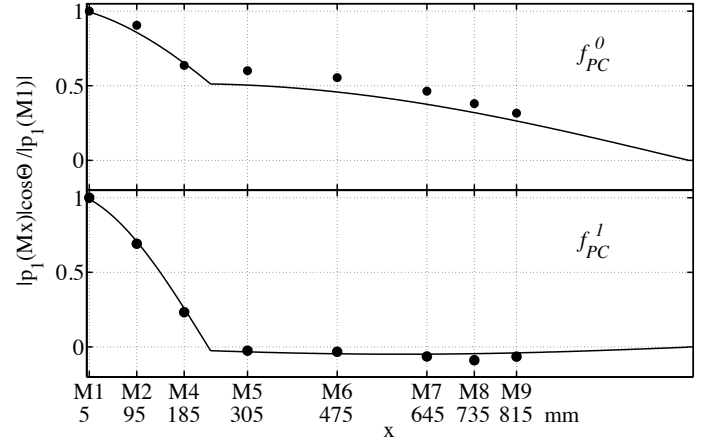


**FIGURE 6.** Analytical (line) and experimental (dots) pressure distributions corresponding to the two first eigenmodes of the system:  $f_{pc}^0 = 180$  Hz and  $f_{pc}^1 = 280$  Hz.

surements under unstable operation match in both cases. The analysis of the structure of these modes also shows that mode 1  $f_{pc}^0 \simeq f_c^0$  features a similar amplitude level in the chamber and in the premixing tube, while mode 2  $f_{pc}^1 \simeq f_p^0$  is characterized by large pressure oscillations in the pre-mixer and reduced fluctuations in the chamber.

The preceding analysis has led to the determination of the first acoustic modes of the combustor and their corresponding structure. It is now interesting to investigate in more details the resonant coupling between the unstable flame and the combustor acoustics at the limit cycle.

#### 4 COUPLING ACOUSTICS, FLOW AND FLAME

It is first possible to evaluate the Rayleigh source term in the acoustic energy balance. This is obtained by integrating Eq.(1) over the reaction volume and over a period of oscillation  $T$  :

$$\mathcal{S}_T = \left\langle \int_V \frac{\gamma-1}{\gamma p_0} p_1 \dot{q}_1 dV \right\rangle_T \quad (16)$$

This term is generally calculated at a single frequency corresponding to the main oscillation peak. In the present study, two unstable modes are observed, it is then preferable to examine this quantity for all frequencies comprised between 0 and 1 kHz. The diagnostics equipping the test bench allow simultaneous recording of the acoustic pressure evolution in the vicinity of the flame region with microphone M5 and fluctuations of the hydroxyl radical emission with a photomultiplier equipped with a narrow band filter. Time traces of these signals are presented in Fig. 7. For premixed flames, fluctuations in the chemiluminescence signal are roughly proportional to heat release rate fluctuations. Following Tran *et al.* [8], the source term  $\mathcal{S}_T$  in Eq. 16 can be evaluated using the cross-spectral densities between the pressure and emission signals with a Welch periodogram method. Results for the source term are plotted in Fig. 8. The positive sign indicates that these two modes at  $f_{pc}^0 = 180$  Hz and  $f_{pc}^1 = 280$  Hz feed acoustic energy to the system. The difference of amplitude between the two peaks already observed on the microphones and chemiluminescence power spectra presented in Fig. 3 is also visible here. The two modes do not provide the same acoustic power. The instability locked on mode 1 associated to the chamber cavity is weaker than that locked on mode 2 associated to the pre-mixer. The influence of the former is however not negligible. It is also shown in Fig. 9 that these modes are present simultaneously and do not correspond to a rapid switch between two limit cycles. The time-frequency diagram shows high values of sound pressure power spectral densities concentrated simultaneously around the two unstable frequencies.

In presence of the acoustic field, the flame responds positively and amplifies acoustic waves leading to a growing instability. When acoustic losses balance this energy input, the system reaches a limit cycle. To gain insight in the amplification mechanism of the flame, it is now relevant to investigate the unsteady flow field evolution in the chamber during unstable operation. A high speed PIV system is set up as described in section 2. The sampling frequency  $f = 15$  kHz is high enough to accurately resolve the two oscillation periods corresponding to the two mode frequencies  $f_{pc}^0$  and  $f_{pc}^1$  over a duration of 0.85 s. This unsteady velocity field is then phase averaged by post-processing. Different techniques can be envisaged for phase averaging at multiple frequencies [31]. This is done here successively at the two distinct forcing frequencies to extract the corresponding dynamics. The pressure signal recorded by microphone M3 located in the

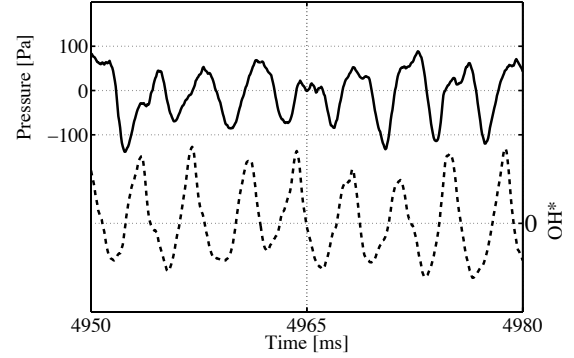


**FIGURE 7.** Simultaneous temporal evolution of the acoustic pressure M5 and OH\* signals in the combustion chamber during unstable operation.

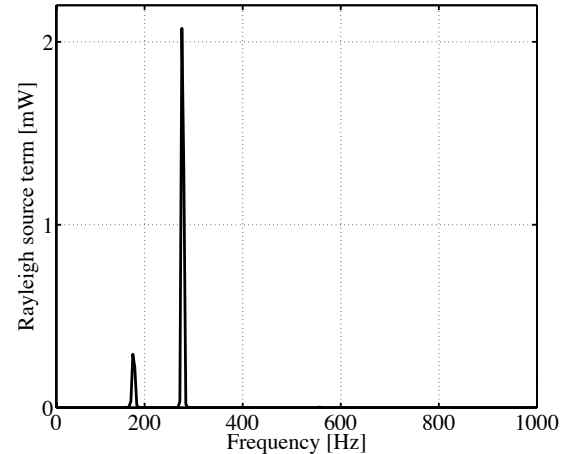


**FIGURE 8.** Rayleigh source term calculated using microphone M5 signal for acoustic pressure and OH\* spontaneous emission for unsteady heat release rate (method described in [8]).

premixer was chosen as a reference to synchronize the phase averaging post-processing. As shown in Fig. 3, this signal features two main peaks at  $f = 180$  and  $280$  Hz. It is then possible to filter this multiple frequencies signal around one peak frequency and used the resulting harmonic filtered signal to synchronize the phase averaging procedure. The same methodology is then repeated for the second peak frequency. The results for the phase conditioned velocity fields related to the first and second acoustic modes are plotted in Fig. 10.

The top images in Fig. 10 display the phase conditioned velocity field at the frequency  $f_{pc}^0 = 180$  Hz at four phases regularly spaced in the oscillation cycle. One can assume that the phase average flame front lies at the limits of this high speed cone. In this case, the flame angle with respect to the mean flow

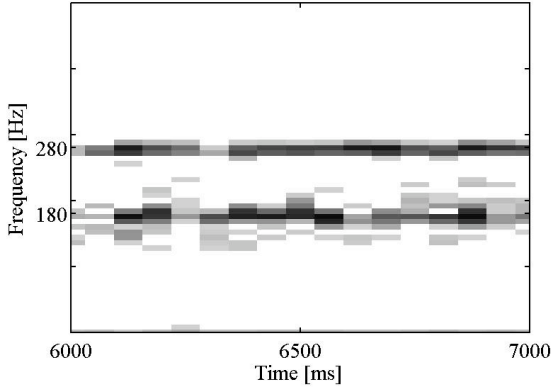


**FIGURE 9.** Time-frequency diagram of the pressure PSD in the combustion chamber during unstable operation. Short duration PSDs are calculated to show that both frequencies are present at the same time.

direction remains constant and the fresh gas penetration cone remains straight during the oscillation cycle. The maximum velocity reached within the cone fluctuates during the cycle and changes the penetration length of the flame in the longitudinal direction. This length reaches its minimum for a phase around  $0^\circ$  and its maximum near  $180^\circ$ . It can be shown that this pulsation follows the acoustic velocity corresponding the first longitudinal mode of the chamber.

The flow in within the flame arms is characterized by a longitudinal bulk oscillation. Images presented on the bottom correspond to phase conditioned velocity fields related to the second eigenmode at the frequency  $f_{pc}^1$ . In this situation, the maximum velocity features wrinkles in the transverse direction during the cycle. The flow in the penetration cone is disturbed in the transverse direction and the flame angle fluctuates near the flame tips. At phase  $0^\circ$ , the flame curvature is oriented toward the exterior of the chamber while it is the reverse direction at phase  $180^\circ$ . At this frequency, the flame length remains relatively constant. So the two acoustic modes interact with the flow and the flame very distinctly in the chamber. Different studies have envisaged swirl number fluctuations to explain oscillations of the flame angle in the transverse direction [32, 33]. It is difficult to conclude if this type of mechanism operates here because the two distinct motions in the longitudinal and transverse directions are associated to distinct acoustic resonances. This requires further investigation of the flow and fame dynamics and conjecture is however proposed to interpret the observed features. The first mode is associated with low frequency pressure fluctuations within the chamber. The corresponding acoustic velocity elongates the flame during the oscillation cycle. The second mode results from large pressure disturbances in the premixing tube which trigger a convective mode at the damp plane characterized by vortices wrinkling the flame front. The two mechanisms are

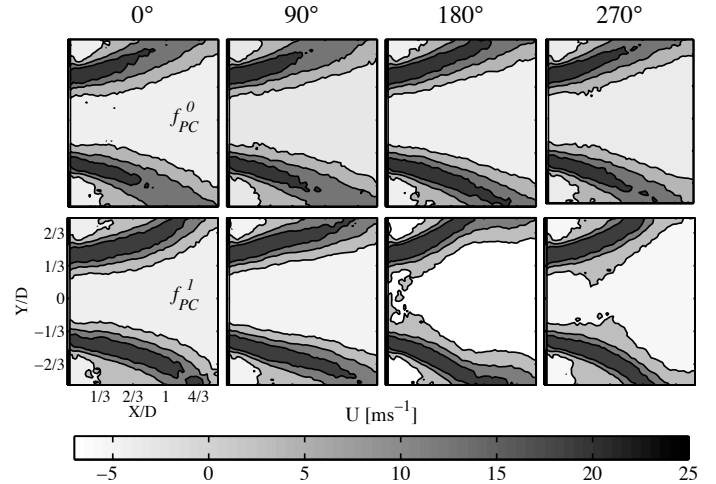


**FIGURE 10.** Phase conditioned velocity fields in the flame region at the first  $f_{pc}^0 = 180$  Hz (top images) and second  $f_{pc}^1 = 280$  Hz (bottom images) unstable modes present simultaneously.

different and superimposed, but both contribute positively to increase the acoustic energy within the system.

Two maps displaying the magnitude of the PSD of the velocity field at the frequencies  $f_{pc}^0$  (left) and  $f_{pc}^1$  (right) are presented in Fig. 11. This is used to examine regions where velocity fluctuations are the highest. These spectral maps show that the fluctuating flow is significantly different for the two unstable modes observed in the combustor. The maximum PSD for mode 1 at  $f_{pc}^1$  is much higher than for mode 2 at  $f_{pc}^0$ . The largest fluctuations occur in the second part of the penetration cone. The flow in the anchoring region does not seem to be perturbed by any of the two modes identified. This has to be confirmed by complementary measurements. The largest velocity fluctuations can be observed in the downstream region for the two modes. Their effects may eventually be coupled since they operate simultaneously in the same region. This remains also to be confirmed by further analysis. It can however be concluded that strong interactions with the flame front and consequently large heat release rate fluctuations are located at the periphery of the fresh gas cone extremities. Interaction with the flame in this region increases the acoustic energy density at two different frequencies by distinct mechanisms. One is associated with a longitudinal motion ( $f_{pc}^0$ ) and the other one with a wrinkling in the transverse direction ( $f_{pc}^1$ ).

## CONCLUSION

The present research investigates combustion instabilities in a swirled combustor open to atmospheric conditions. High speed PIV, acoustic pressure and flame emission measurements were carried out to characterize the acoustic behavior of the combus-

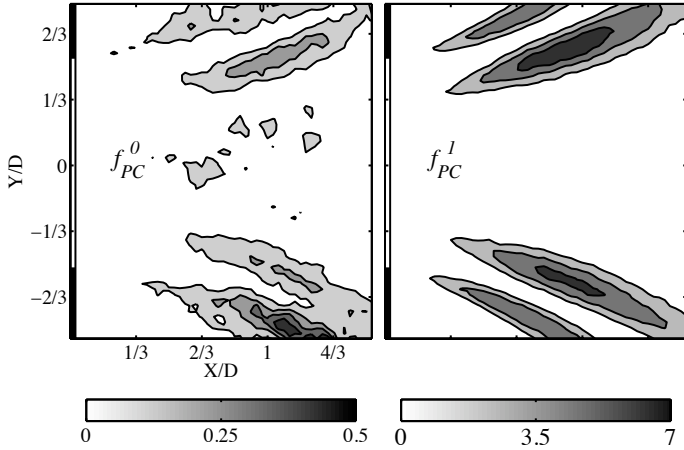


**FIGURE 11.** Two dimensions PSD magnitude of the velocity field at the frequencies  $f_{pc}^0$  (left) and  $f_{pc}^1$  (right). Distances are normalized by the pre-mixer diameter  $D=3$  cm

tor and its coupling with the flow and the combustion process. The acoustic modes were determined using a low-order model taking into account realistic acoustic boundary conditions. This was used to analyze the structure of the first acoustic modes of the combustor in the low frequency 0-500 Hz band. The Rayleigh source term was evaluated indicating that the acoustic source term in the chamber is the sum of two components associated with two eigenfrequencies present simultaneously. The first corresponds to the chamber first cavity mode and the second is the pre-mixer first cavity mode. The coupling mechanism between acoustics, flow and flame was examined at these frequencies using high speed PIV and a phase averaging procedure. This analysis showed distinct flame responses at the two non-harmonically related frequencies, highlighting two different contributions feeding acoustic energy within the system and operating simultaneously. A deeper analysis of these mechanisms is a work in progress.

## ACKNOWLEDGMENT

Ammar Lamraoui benefits from a PhD grant from *Fondation de Recherche pour l'Aéronautique et l'Espace (FNRAE)*. The results are issued from studies supported by FNRAE in the framework of the BRUCO project (*BRUit de COmbustion*) dedicated to combustion noise analysis.

## NOMENCLATURE

$A^\pm$  Pressure waves amplitude in the positive/negative direction  
 $\bar{c}$  Sound celerity [ $\text{m s}^{-1}$ ]  
 $\mathcal{E}$  Acoustic energy density [ $\text{W m}^{-3}$ ]

$f_c^i$   $i$ -th eigenfrequency associated with the combustion chamber  
 $f_p^i$   $i$ -th eigenfrequency associated with the pre-mixer tube  
 $f_{pc}^i$   $i$ -th eigenfrequency of the combustor  
 $k$  Wave number [ $\text{m}^{-1}$ ]  
 $L$  Length [mm]  
 $M$  Mach number  
 $\dot{m}$  Mass flow rate [ $\text{g s}^{-1}$ ]  
 $p$  Acoustic pressure [Pa]  
 $\dot{q}$  Heat release rate [ $\text{W m}^{-2} \text{s}^{-1}$ ]  
 $R$  Acoustic reflection coefficient  
 $\mathcal{S}_T$  Rayleigh source term [W]  
 $T$  Temperature [K] or oscillation period [s]  
 $u$  Acoustic velocity [ $\text{m s}^{-1}$ ]  
 $Z$  Characteristic impedance [ $\text{kg m}^{-2} \text{s}^{-1}$ ]  
 $\alpha$  Fuel staging ratio [%]  
 $\gamma$  Specific heat capacity ratio  
 $\delta$  End correction [mm]  
 $\Xi$  Acoustic interaction index  
 $\bar{\rho}$  Density [ $\text{kg m}^{-3}$ ]  
 $\Phi$  Phase of the reflection coefficient [rad]  
 $\omega$  Pulsation [Hz]

## Subscripts

0 Mean value  
1 Fluctuating part  
c Combustion chamber  
p Premixer  
pc The whole combustor

## REFERENCES

- [1] Poinot, T., and Veynante, D., 2005. *Theoretical and Numerical Combustion (2nd Edition)*. Edwards.
- [2] Chu, B.-T., 1965. "On the energy transfer to small disturbances in fluid flow (part i)". *Acta Mechanica*, **1**, pp. 215–234.
- [3] Cantrell, R. H., and Hart, R. W., 1964. "Interaction between sound and flow in acoustic cavities: Mass, momentum, and energy considerations". *The Journal of the Acoustical Society of America*, **36**(4), 04, pp. 697–706.
- [4] Myers, M., 1991. "Transport of energy by disturbances in arbitrary steady flows". *Journal of Fluid Mechanics*, **226**, pp. 383 – 400.
- [5] Nicoud, F., and Poinot, T., 2005. "Thermoacoustic instabilities: Should the rayleigh criterion be extended to include entropy changes?". *Combustion and Flame*, **142**(1-2), pp. 153–159.
- [6] Karimi, N., Brear, M. J., and Moase, W. H., 2008. "Acoustic and disturbance energy analysis of a flow with heat com-

- munication”. *Journal of Fluid Mechanics*, **597**, pp. 67 – 89.
- [7] Nicoud, F., and Wieczorek, K., 2009. “About the zero mach number assumption in the calculation of thermoacoustic instabilities”. *International Journal of Spray and Combustion Dynamics*, **1**(1), pp. 67–112.
- [8] Tran, N., Ducruix, S., and Schuller, T., 2009. “Damping combustion instabilities with perforates at the premixer inlet of a swirled burner”. *Proceedings of the Combustion Institute*, **32**(2), pp. 2917 – 2924.
- [9] Salikuddin, M., and Zinn, B., 1980. “Adaptation of the impedance tube technique for the measurement of combustion process admittances”. *Journal of Sound and Vibration*, **68**(1), pp. 119 – 132.
- [10] Eldredge, J., and Dowling, A., 2003. “The absorption of axial acoustic waves by a perforated liner with bias flow”. *Journal of Fluid Mechanics*, **485**, pp. 307–335.
- [11] Lamarque, N., and Poinsot, T., 2008. “Boundary conditions for acoustic eigenmode computations in gas turbine combustion chambers”. *AIAA Journal*, **46**(9), pp. 2282–2292.
- [12] Schuller, T., Tran, N., Noiray, N., Durox, D., Ducruix, S., and Candel, S., 2009. “The role of nonlinear acoustic boundary conditions in combustion/acoustic coupled instabilities”. In Proceedings of the ASME Turbo Expo, Vol. 2, pp. 325–339.
- [13] Bothien, M. R., Moeck, J. P., and Paschereit, C. O., 2008. “Active control of the acoustic boundary conditions of combustion test rigs”. *Journal of Sound and Vibration*, **318**(4-5), pp. 678 – 701.
- [14] Lamraoui, A., Richecoeur, F., Schuller, T., and Ducruix, S., 2011. “A methodology for on the fly acoustic characterization of the feeding line impedances in a turbulent swirled combustor”. *Journal of Engineering for Gas Turbines and Power*, **133**(1), 01, pp. 011504–7.
- [15] Durox, D., Schuller, T., Noiray, N., Birbaud, A. L., and Candel, S., 2009. “Rayleigh criterion and acoustic energy balance in unconfined self-sustained oscillating flames”. *Combustion and Flame*, **156**(1), pp. 106–119.
- [16] Tran, N., Ducruix, S., and Schuller, T., 2009. “Passive control of the inlet acoustic boundary of a swirled burner at high amplitude combustion instabilities”. *Journal of Engineering for Gas Turbines and Power*, **131**(5), 09, pp. 051502–7.
- [17] Moeck, J., and Paschereit, C., 2010. “Nonlinear interactions of multiple linearly unstable thermoacoustic modes”. In Int’l Summer School and Workshop on Non-Normal and Nonlinear Effects in Aero and Thermoacoustics, Technische Universität München.
- [18] Schuermans, B., Bellucci, V., and Paschereit, C. O., 2003. “Thermoacoustic modeling and control of multi burner combustion systems”. *ASME Conference Proceedings*, **2003**(36851), 01, pp. 509–519.
- [19] Stow, S. R., and Dowling, A. P., 2009. “A time-domain network model for nonlinear thermoacoustic oscillations”. *Journal of Engineering for Gas Turbines and Power*, **131**(3), pp. 1 – 10.
- [20] Gutmark, E., Wilson, K., Parr, T., and Schadow, K., 1992. “Feedback control of multi-mode combustion instability”. In AIAA paper 92-0778.
- [21] Dunstan, W. J., Bitmead, R. R., and Savaresi, S. M., 2001. “Fitting nonlinear low-order models for combustion instability control”. *Control Engineering Practice*, **9**(12), pp. 1301 – 1317.
- [22] Riley, A., Park, S., Dowling, A., Evesque, S., and Annaswamy, A., 2004. “Advanced closed-loop control on an atmospheric gaseous lean-premixed combustor”. *Journal of Engineering for Gas Turbines and Power*, **126**(4), pp. 708 – 716.
- [23] Culick, F., Lin, W., Jahnke, C., and Sterling, J., 1991. “Modeling for active control of combustion and thermally driven oscillations”. *Proceedings of the American Control Conference*, **3**, pp. 2939 – 2948.
- [24] Kabiraj, L., Saurabh, A., Wahi, P., and Sujith, R., 2010. “Experimental study of thermoacoustic instability in ducted premixed flames: Periodic, quasi-periodic and chaotic oscillations”. In Int’l Summer School and Workshop on Non-Normal and Nonlinear Effects in Aero and Thermoacoustics, Technische Universität München.
- [25] Noiray, N., Durox, D., Schuller, T., and Candel, S., 2008. “A unified framework for nonlinear combustion instability analysis based on the flame describing function”. *Journal of Fluid Mechanics*, **615**, pp. 139 – 167.
- [26] Boudy, F., Durox, D., Schuller, T., and Candel, S., 2011. “Nonlinear mode triggering in a multiple flame combustor”. *Proceedings of the Combustion Institute*, **33**(1), pp. 1121–1128.
- [27] Balachandran, R., Dowling, A., and Mastorakos, E., 2008. “Non-linear response of turbulent premixed flames to imposed inlet velocity oscillations of two frequencies”. *Flow, Turbulence and Combustion*, **80**(4), pp. 455 – 487.
- [28] Ducruix, S., Schuller, T., Durox, D., and Candel, S., 2003. “Combustion dynamics and instabilities: Elementary coupling and driving mechanisms”. *Journal of Propulsion and Power*, **19**(5), pp. 722 – 734.
- [29] Dioc, N., 2005. “Etude expérimentale des mécanismes d’instabilité dans un brûleur à injection étagée, application aux turbines à gaz”. PhD thesis, Ecole Centrale Paris.
- [30] Munjal, M., 1987. *Acoustics of ducts and mufflers*. John Wiley and Sons.
- [31] Steinberg, A., Boxx, I., Stöhr, M., Carter, C., and Meier, W., 2010. “Flow-flame interactions causing acoustically coupled heat release fluctuations in a thermo-acoustically unstable gas turbine model combustor”. *Combustion and*

*Flame*, **157**(12), pp. 2250 – 2266.

- [32] Hirsch, C., Fanaca, D., Reddy, P., Polifke, W., and Sattelmayer, T., 2005. “Influence of the swirler design on the flame transfer function of premixed flames”. In Proceedings of the ASME Turbo Expo 2005, Vol 2, pp. 151–160.
- [33] Palies, P., Durox, D., Schuller, T., and Candel, S., 2010. “The combined dynamics of swirler and turbulent premixed swirling flames”. *Combustion and Flame*, **157**(9), pp. 1698–1717.